processes

MDPI

Article

Target Tracking Two Degrees of Freedom State Feedback Control for Continuous Flow Microfluidic Chips Temperature Controller

Yuqi Jiang [1], Yang Liu [2], Yuxiong Xue [2], Wei Jiang [1,*] and Seiji Hashimoto [3]

[1] Yangzhou Polytechnic Institute, 199 Huayangxi Road, Yangzhou 225127, China; jiangyuqiygy@outlook.com
[2] College of Electrical, Energy and Power Engineering, Yangzhou University, 88 Daxue South Road, Yangzhou 225009, China; liuy@ypi.edu.cn (Y.L.); xueyx@ypi.edu.cn (Y.X.)
[3] Division of Electronics and Informatics, Gunma University, Kiryu 376-8515, Japan; seijihashimoto@gunma-u.jp.com
* Correspondence: jiangw@ypi.edu.cn

Abstract: Microfluidic chips represent a cutting-edge technology for manipulating fluids within micrometer-scale spaces and are gradually becoming a new favorite platform in life science research. Precise and fast zonal temperature control is essential for accelerating biological experiments. However, current multi-channel temperature controllers typically rely on multiple channel sets to achieve single set-point control, which results in discrepancies between the fluid temperature distribution and sensor temperature due to the distributed temperature field in the fluid channel. To estimate the actual temperature and implement gradient temperature control, this paper introduces an extension of the target tracking (TT) two degrees of freedom (2DOF) state feedback control (SFC) method, followed by a presentation of simulation and experimental results. Through comparisons with an enhanced PID system in both simulation and experimentation, the paper demonstrates an 8.96% reduction in the maximum temperature difference across different regions and a 27.89% decrease in the time taken to reach various temperatures. This solution effectively addresses the existing challenges in temperature control for microfluidic chips, offering a more precise and stable control within the desired temperature range.

Keywords: temperature control; 2DOF; SFC; MIMO

check for updates

Citation: Jiang, Y.; Liu, Y.; Xue, Y.; Jiang, W.; Hashimoto, S. Target Tracking Two Degrees of Freedom State Feedback Control for Continuous Flow Microfluidic Chips Temperature Controller. *Processes* **2024**, *12*, 1108. https://doi.org/10.3390/pr12061108

Received: 25 April 2024
Revised: 19 May 2024
Accepted: 25 May 2024
Published: 28 May 2024

Copyright: © 2024 by the authors. Licensee MDPI, Basel, Switzerland. This article is an open access article distributed under the terms and conditions of the Creative Commons Attribution (CC BY) license (https://creativecommons.org/licenses/by/4.0/).

1. Introduction

Microfluidic chips, since their inception, have transformed the landscape of life sciences with their remarkable capabilities. These chips offer high efficiency in mass and heat transfer, enabling rapid and precise control over biochemical reactions. Their design facilitates minimal sample consumption, which is particularly beneficial for experiments involving scarce or valuable biological materials. The high integration level of microfluidic chips allows for the miniaturization and parallelization of complex laboratory processes onto a single chip, thereby enhancing experimental throughput and efficiency [1–3].

Moreover, the swift detection capabilities of microfluidic chips have accelerated the pace of scientific discovery. The ability to perform real-time monitoring and analysis on a microscale contributes to their growing popularity in various research areas, including drug discovery, disease modeling, and environmental sensing [4,5].

Temperature is a pivotal parameter in the growth and development of organisms. It significantly influences enzymatic activities, cellular metabolism, and reaction kinetics, making temperature control an indispensable aspect of biological experiments [6,7]. Accurate temperature regulation ensures that experimental conditions are maintained consistently, which is crucial for obtaining reliable and reproducible results.

The primary methods of temperature control in microfluidic systems are microreactor cavity-based control and continuous flow control [8]. In microreactor cavity-based control,

the reaction solution is held stationary within a cavity, and its temperature is modulated by external heating and cooling devices. This method allows for precise control over the reaction conditions, facilitating the achievement of desired outcomes in various chemical and biological processes.

Conversely, continuous flow control involves the steady passage of the solution through a series of temperature zones within the microfluidic chip. This method enables dynamic temperature adjustments that can be tailored to the specific requirements of the reaction as it progresses. The flexibility offered by continuous flow control is particularly advantageous for complex assays that demand multiple steps or varying conditions [9].

Continuous flow microfluidic chips present several advantages, such as high throughput, elimination of cooling requirements, and the capability for continuous measurement. These features make them highly suitable for applications where process control and optimization are critical, such as in industrial and clinical settings. Due to these benefits, continuous flow microfluidic chips are increasingly replacing microreactor cavity-based microfluidic chips in various scientific and medical applications [7].

Kopp et al. were pioneers in the development and application of continuous flow microfluidic chips for polymerase chain reaction (PCR) processes. They utilized three heating blocks controlled by a PID (proportional–integral–derivative) controller to achieve and maintain three distinct temperatures required for PCR. However, this method had its limitations as it controlled only the temperature of the external heating blocks and not the actual liquid temperature within the microchannels, which could lead to inaccuracies in the experimental outcomes [10].

In an effort to address this issue, Liu et al. proposed an innovative open-loop temperature control system. This system was based on multi-parameter identification and employed a model of the microfluidic chip to infer the actual temperature of the fluid through temperature detection. This approach allowed for the control of the actual fluid temperature within a specific range, offering a significant advancement over previous methods. Nonetheless, in practical applications, variations in flow rate and fluid properties could lead to parameter variations, weakening the system's anti-interference ability and hindering the accurate prediction of the actual fluid temperature. Moreover, the open-loop control lacked an automatic temperature correction mechanism [11].

Ulep et al. introduced a point of care testing platform based on droplet loop-mediated isothermal amplification (LAMP). This design overcame some of the previous limitations by directly inserting a temperature probe into the fluid, which allowed for accurate temperature measurement and enhanced the robustness and accuracy of temperature control through closed-loop control. However, this method, while effective for static fluids, was not suitable for flowing fluids and suffered from a slower response time [12].

Ren et al. further advanced the field by implementing an improved PID-Fuzzy control strategy. This strategy involved adjusting the PID parameters during different stages of operation, which improved the response time and robustness of the system to some extent. However, the independent control of multiple temperature control modules in close proximity could lead to temperature fluctuations due to mutual interference, indicating that there was still room for further improvement in temperature control systems for microfluidic chips [13].

To optimize temperature control in microfluidic chips, this paper proposes a multi-channel temperature control system, Figure 1, based on target tracking, specifically a 2DOF state feedback control for a MIMO temperature controller, designed to meet the control requirements for different positions and varying temperatures across the chip. The proposed system first establishes the system model that relates heater voltage to the actual liquid temperature using a step response. Subsequently, an observer is designed to estimate the actual liquid temperature by measuring nearby temperatures. The system is decoupled, and temperature control is achieved through state-space feedback. Built on this foundation, a target tracking system is implemented to ensure stable gradient control, and feed-forward control is incorporated to expedite the system's response.

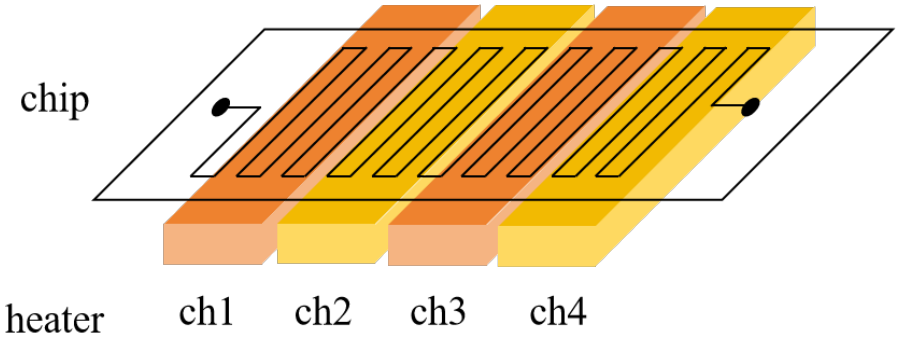

Figure 1. Continuous flow microfluidic chips.

This paper assesses the effectiveness of the proposed system by comparing its performance to that of an improved PID (proportional–integral–derivative) system through both simulation and experimentation. The experimental results demonstrate an 18% improvement in response time and a 23% reduction in overshoot. Additionally, the system achieves an 8.96% reduction in the maximum temperature difference across different regions and a 27.89% decrease in the time required to reach various temperatures. The proposed system effectively addresses the challenges faced by current temperature control methods in microfluidic chips, providing a more effective solution for precise temperature control and stability within the targeted temperature range.

2. Heating System Plant Identification

System identification is essential and effective tool in control engineering to understand the behavior of dynamic systems. It involves developing a mathematical model that represents the input–output relationship of a system based on measured data.

The general approach to system identification includes the following steps:

Data Collection: to gather input–output data from the system under test. These data can be obtained through experiments or recorded from the system's operation.
Model Structure Selection: to choose an appropriate model structure that represents the system's dynamics. Common structures include linear models such as ARX (AutoRegressive with exogenous inputs), transfer functions, or state-space models.
Parameter Estimation: to use the collected data to estimate the parameters of the chosen model structure. Techniques such as least squares, maximum likelihood, or recursive algorithms can be employed.
Model Validation: to validate the identified model by comparing its predictions with additional data not used in the parameter estimation step. This ensures the model's accuracy and generalizability.
Model Refinement: if the model does not adequately represent the system, refine the model structure or re-estimate the parameters until an acceptable model is obtained.

2.1. The Temperature Control System

In the temperature control system, the controller generates the trigger pulses for the thyristor, which in turn supplies cycles of ac voltage to the heating rod. Concurrently, the temperature sensor converts the temperature signal into a voltage signal and sends it back to the controller, forming a close-loop system. This feedback mechanism adjusts the trigger signal accordingly. Consequently, to maintain a stable temperature, precise cycle control of the supply voltage is essential.

Currently, model-based control algorithms are extensively and profoundly utilized, with their effectiveness being directly proportional to the depth of understanding of the controlled system. However, due to various factors, obtaining accurate models of the plant can be challenging, and these models may evolve over time. The application of system identification techniques serves as an effective method for acquiring the mathematical models of such systems. Given the crucial role of servo valves in electro-hydraulic servo

systems, it is especially important to identify and model the dynamic characteristics of these valves.

Generally, a temperature control plant can be approximated as a first-order inertial element. However, in practice, this system can be more accurately described as a first-order inertial plus lag element, given the time delay that exists between the temperature reading from the sensor and the actual temperature of the liquid. A simple heating system consisting of a heating rod and a thermal mass. The system can be modeled as a first-order inertial element with a pure lag.

The energy balance for the heating rod and thermal mass system can be represented as follows:

$$Q(t) = m \cdot c \cdot \frac{dT(t)}{dt} + V(t) \tag{1}$$

where $Q(t)$ is the heat input from the heating rod, m is the mass of the thermal mass, c is the specific heat capacity, $T(t)$ is the temperature of the thermal mass, and $V(t)$ represents the heat loss due to lag.

Applying the Laplace transform to the energy balance equation, we obtain:

$$Q(s) = m \cdot c \cdot s \cdot T(s) - m \cdot c \cdot T(0) + V(s) \tag{2}$$

Assuming zero initial conditions, $T(0) = 0$, the equation simplifies to:

$$Q(s) = m \cdot c \cdot s \cdot T(s) + V(s) \tag{3}$$

The transfer function $G(s)$ is defined as the ratio of the output $T(s)$ to the input $Q(s)$:

$$G(s) = \frac{T(s)}{Q(s)} \tag{4}$$

Assuming $V(s)$ has the same time constant τ as $T(s)$, such that $V(s) = \tau \cdot s \cdot T(s)$, the transfer function becomes:

$$G(s) = \frac{1}{m \cdot c \cdot s + \tau \cdot s} \tag{5}$$

Simplifying, we obtain the final transfer function:

$$G(s) = \frac{1}{s \cdot (m \cdot c + \tau)} \tag{6}$$

In practical applications, the transfer function may be more complex and can be augmented by incorporating additional time delays to accurately describe the dynamic behavior of the system. The final transfer function represents the relationship between the heating input $Q(s)$ and the temperature response $T(s)$,

$$\frac{K}{Ts + 1} e^{-\tau s}, \tag{7}$$

where K is the temperature transfer coefficient, T is the time constant, which is a combination of the system's thermal resistance and thermal capacity, and τ is delay time.

This transfer function can be used to analyze and design temperature control systems, determining their stability and response characteristics.

2.2. System Identification Method

Perform a pull-inverse transformation to obtain the following equation:

$$y(t) = Ke^{-(t-L)/T} + w(t), \tag{8}$$

where $w(t)$ is the noise.

Equation (8) can be converted to

$$e^{-(t-L)/T} = \frac{y(t)}{K} + \frac{w(t)}{K}, \tag{9}$$

Integrate Equation (8) to obtain the following:

$$\int_0^\tau y(t)dt = K[T - Te^{-(t-L)/T}] + \int_0^\tau w(t)dt, \tag{10}$$

Substituting Equation (9) into Equation (10) results in

$$\int_0^\tau y(t)dt = K[T - T\frac{y(\tau)}{K}] + w(\tau) + \int_0^\tau w(t)dt \tag{11}$$

Suppose $A(\tau) = \int_0^\tau y(t)dt$, $\delta(\tau) = w(\tau) + \int_0^\tau w(t)dt$. Therefore, Equation (11) can be written as a system of linear equations.

$$\Psi\theta = \Gamma + \Delta \quad \tau \geq L, \tag{12}$$

where

$$\begin{gathered} \theta = \begin{bmatrix} KT \\ T \end{bmatrix}, \Psi = \begin{bmatrix} 1 & -y[mT_s] \\ 1 & -y[(m+1)T_s] \\ \vdots & \vdots \\ 1 & -y[(m+n)T_s] \end{bmatrix}, \\ \Gamma = \begin{bmatrix} A[mT_s] \\ A[(m+1)T_s] \\ \vdots \\ A[(m+n)T_s] \end{bmatrix}, \Delta = \begin{bmatrix} -\delta[mT_s] \\ -\delta[(m+1)T_s] \\ \vdots \\ -\delta[(m+n)T_s] \end{bmatrix}, \end{gathered} \tag{13}$$

where T_s is the discrete sampling time, and mT_s must be greater than or equal to L. Finally, the estimation of θ that can be obtained using the least squares method is

$$\theta = (\Psi^T\Psi)^{-1}\Psi^T\Gamma, \tag{14}$$

The parameters can be found by Equation (14). K, T is

$$\begin{bmatrix} K \\ T \end{bmatrix} = \begin{bmatrix} \theta_1/\theta_2 \\ \theta_2 \end{bmatrix}, \tag{15}$$

where θ_1 and θ_2 represent the first and second components of $\hat{\theta}$.

Next, we obtain the value of L. First, the following equation is obtained by integrating $ty(t)$

$$\int_0^\tau ty(t)dt = K[T^2 + TL - T\tau e^{-(t-L)/T} - T^2e^{-(t-L)/T}] + \int_0^\tau w(t)dt, \tag{16}$$

Substituting Equation (9) into Equation (16),

$$\int_0^\tau y(t)dt = K[T^2 + TL - T\tau\frac{y(\tau)}{K} - T^2\frac{y(\tau)}{K}] + (T\tau + T^2)w(\tau) + \int_0^\tau w(t)dt \tag{17}$$

Suppose $A(\tau) = \int_0^\tau ty(t)dt$, $\delta(\tau) = (T\tau + T^2)w(\tau) + \int_0^\tau w(t)dt$. Therefore, Equation (17) can be written as a system of linear equations.

$$\Psi\theta = \Gamma + \Delta \quad \tau \geq L, \tag{18}$$

where

$$\theta = \begin{bmatrix} T \\ T^2 \\ KT(T+L) \end{bmatrix}, \Psi = \begin{bmatrix} -mT_s y[mT_s] & -y[mT_s] & 1 \\ -(m+1)T_s y[mT_s] & -y[(m+1)T_s] & 1 \\ \vdots & \vdots & \vdots \\ -(m+n)T_s y[mT_s] & -y[(m+n)T_s] & 1 \end{bmatrix},$$
$$\Gamma = \begin{bmatrix} A[mT_s] \\ A[(m+1)T_s] \\ \vdots \\ A[(m+n)T_s] \end{bmatrix}, \Delta = \begin{bmatrix} -\delta[mT_s] \\ -\delta[(m+1)T_s] \\ \vdots \\ -\delta[(m+n)T_s] \end{bmatrix}, \tag{19}$$

where T_s is the discrete sampling time, and mT_s must be greater than or equal to L. Finally, the estimation of θ that can be obtained using the least squares method is

$$\theta = (\Psi^T \Psi)^{-1} \Psi^T \Gamma, \tag{20}$$

By combining Equation (20) with K and T obtained by Equation (15), the value of L can be found as

$$L = \theta_3 / (KT) - T, \tag{21}$$

where θ_3 represent the third components of $\hat{\theta}$.

Finally, the identification parameters of the first-order inertial differential pure hysteresis model can be obtained by Equations (15) and (21).

2.3. System Identification Result

Before customizing the microfluidic chip for specific testing applications, it is essential to construct a reliable temperature control system. This system serves to validate not only the effectiveness of the temperature regulation algorithm but also the overall thermal performance of the chip under various conditions.

The preliminary stage involves setting up a temperature control system that emulates the operational environment of the microfluidic chip. As shown in Figure 2, the configuration includes four heating blocks positioned beneath the chip, designed to mimic the thermal dynamics during actual chip usage.

The experimental setup, as depicted in Figure 3, consists of four aluminum blocks, each playing a critical role in the temperature control process. These blocks are equipped with two heating rods and a temperature sensor, allowing for precise heating and monitoring of the thermal state within each block.

Each aluminum block is designated as ch1, ch2, ch3, and ch4, corresponding to their position and function within the system. The voltage applied to the heating rods is carefully controlled, and the temperature data collected by the sensors are digitized and transmitted to a computer system. This computer acts as the central monitoring unit, facilitating real-time control and adjustment of the temperature parameters through a dedicated temperature controller.

To engineer a precise control system capable of meeting the stringent requirements of microfluidic chip testing, system identification becomes a crucial first step. This process involves the analysis of the system's dynamic behavior in response to various inputs and the development of a mathematical model that accurately represents this behavior.

During the experiment, a step voltage of 1 V was individually applied to the heating rods of each of the four channels, and the temperature signals from the sensors in these channels were recorded simultaneously. The temperature signal recorded by the sensor in channel ch1 upon the application of voltage is depicted in Figure 4.

Implementing requirements for adequacy and causality in practice presents significant challenges, particularly when configuring high-dimensional MIMO processes. To address

these challenges, research efforts have predominantly concentrated on double-input double-output (DIDO) processes.

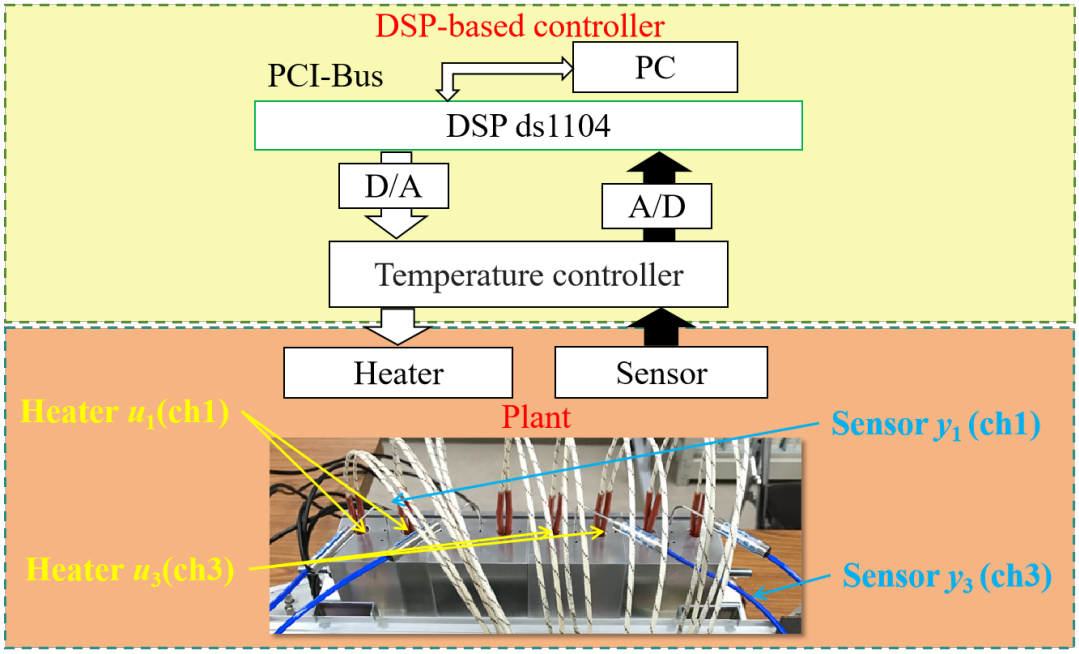

Figure 2. Test prototype structure.

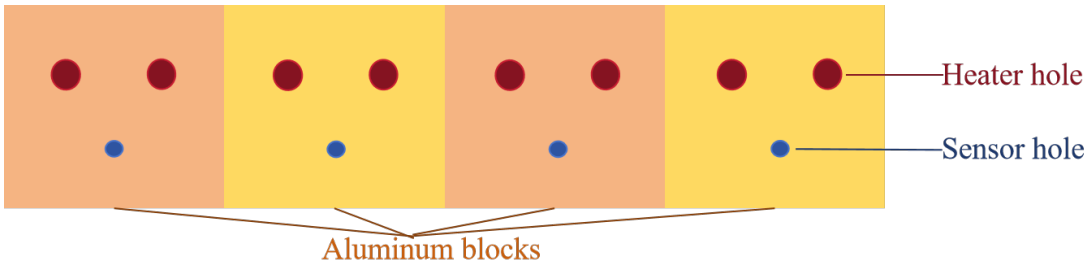

Figure 3. Heater and sensor location.

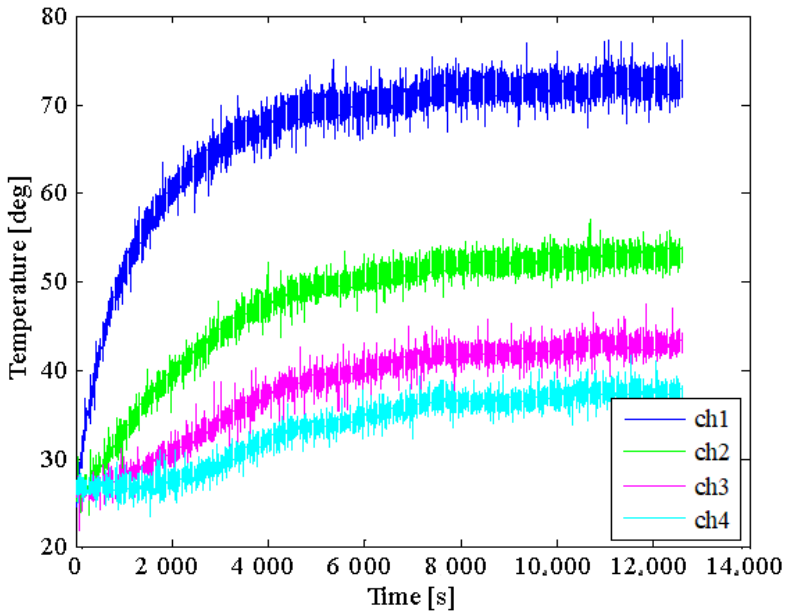

Figure 4. Step response of ch1 step input.

In this particular design, channels ch1 and ch3 have been chosen for study. The linear model for these channels can be approximated as a first-order system with time delay. The formula for calculating the parameters is presented below.

$$\begin{bmatrix} \frac{4.52}{1211s+1}e^{-25s} & \frac{1.91}{1211s+1}e^{-600s} \\ \frac{1.67}{3984s+1}e^{-400s} & \frac{4.52}{1639s+1}e^{-30s} \end{bmatrix}, \tag{22}$$

The Bode diagram of the system is shown in Figure 5.

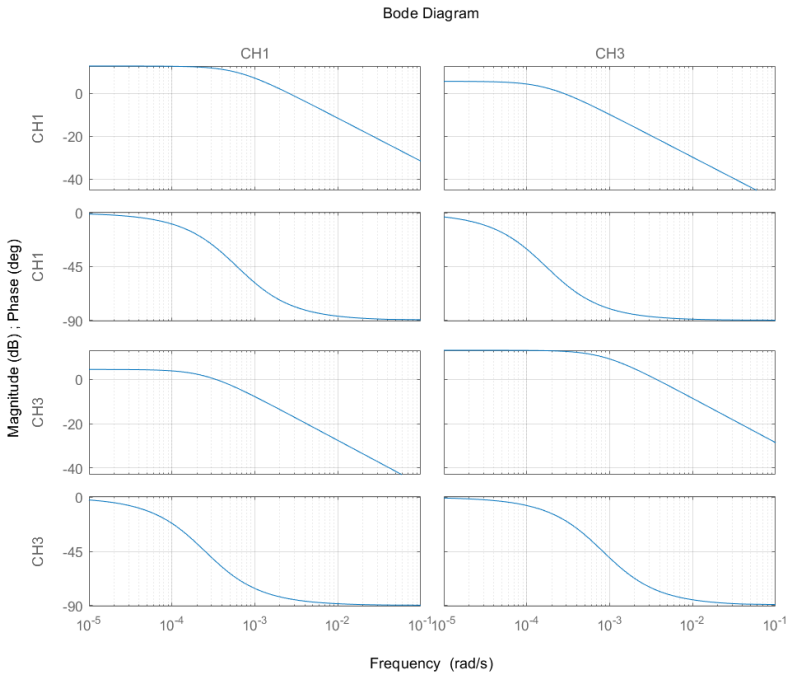

Figure 5. Bode of plant.

3. Target-Follow State Space Model

Subsequently, the composition of the system will be detailed across five key components: system decoupling, state observer design, integral negative feedback design, tracking link design, and feedforward design.

3.1. System Decoupling

In the realm of control systems engineering, the phenomenon of overshoot can lead to instability and inefficiency in system performance. Overshoot occurs when the system's response exceeds the desired set point before it settles down. This can be particularly problematic in precision applications, such as in microfluidic chip temperature control, where accurate and stable temperature zones are crucial for biological experiments and chemical reactions. To address the issue of overshoot stemming from system coupling, a strategic approach is to decouple the system. System coupling refers to the interdependencies between different parts of a system, which can lead to complex and challenging control scenarios. Decoupling is the process of reducing these interdependencies, allowing for the independent control of each subsystem. This simplifies the control design and improves the overall system stability and performance. The initial step in decoupling is to analyze the system and identify its individual components, which in this case are the subsystems that make up the whole. As detailed in the previous section of the paper, the system under study has been delineated into four inertial delay links. These links represent different parts of the system that contribute to the overall temperature control behavior. By treating each link as a separate subsystem, the complexity of the entire system can be more effectively managed. Once the system has been broken down into these four inertial delay links, each

subsystem can be described using a state-space model. State-space representation is a mathematical framework that allows for the analysis of complex systems by representing them as a set of first-order differential equations. This approach is particularly useful for linear time-invariant (LTI) systems, which are common in control theory. The state-space equation for each subsystem can be formulated as follows:

$$\begin{aligned} \dot{x}(t) &= A\dot{x}(t) + Bu(t), \\ y(t) &= C\dot{x}(t), \end{aligned} \tag{23}$$

in this system, where $\dot{(}x)(t)$ represents the time derivative of the state vector $x(t)$, $A = \begin{bmatrix} -1/T \end{bmatrix}$ is the state matrix, $B = \begin{bmatrix} K/T \end{bmatrix}$ is the input matrix, $u(t)$ is the control input vector, $y(t)$ is the output vector, and $C = \begin{bmatrix} 1 \end{bmatrix}$ is the output matrix. The state vector $\dot{x}(t)$ includes the states of the system, such as the temperatures and energy inputs at each of the four inertial delay links.

Next, the subsystems are combined diagonally to obtain a complete decoupled system.

$$\begin{gathered} A = \begin{bmatrix} A_{11} & 0 & 0 & 0 \\ 0 & A_{21} & 0 & 0 \\ 0 & 0 & A_{12} & 0 \\ 0 & 0 & 0 & A_{22} \end{bmatrix}, B = \begin{bmatrix} B_{11} & 0 \\ B_{21} & 0 \\ 0 & B_{12} \\ 0 & B_{22} \end{bmatrix}, \\ C = \begin{bmatrix} C_{11} & C_{21} & 0 & 0 \\ 0 & 0 & C_{21} & C_{22} \end{bmatrix}, \end{gathered} \tag{24}$$

3.2. State Observer

The primary objective of this system is to regulate the temperature of the liquid within the microfluidic chip. Achieving this level of control is paramount, as it directly impacts the efficiency and accuracy of experiments conducted on the chip. However, direct measurement of the internal liquid temperature presents a significant challenge due to the small scale and complex geometry of microfluidic channels.

To circumvent the limitations associated with direct temperature measurement, an observer is employed within the control system. This observer is designed to estimate the actual temperature of the liquid within the microfluidic chip. It utilizes the input voltage applied to the heating elements and the temperature readings from peripheral sensors to infer the internal liquid temperature. This approach is particularly useful when direct measurement is not feasible, as is often the case with microfluidic systems.

In the context of this experiment, since no microfluidic chip is installed, the default measured temperature from the peripheral sensors is assumed to be equivalent to the actual temperature of the system. This assumption allows for the initial calibration and testing of the observer design. The observer utilizes the system parameters that have been previously described and validated, ensuring a robust estimation of the liquid temperature.

Based on the observer's design and the system parameters, the transfer function of the control system is modified accordingly. This modification ensures that the control algorithm accounts for the estimated temperature, allowing for precise regulation of the liquid's thermal state. The updated transfer function is essential for the implementation of feedback control strategies that rely on accurate temperature measurements.

The incorporation of an observer in the control system, as detailed by Share Pasand and Ahmadi [14], is a significant advancement in the field of microfluidic temperature control. It allows for the extension of control theory to complex systems where direct measurement is either impractical or impossible.

The objective is to design an observer of the following form:

$$\dot{\hat{x}}(t) = A\hat{x}(t) + Bu(t) + L(y(t) - C\hat{x}(t)) \tag{25}$$

where $\hat{x}(t)$ is the estimated state vector and L is the observer gain matrix to be determined.

The error $e(t)$ between the actual state and the estimated state is defined as follows:

$$e(t) = x(t) - \hat{x}(t) \tag{26}$$

The dynamics of the error can be expressed as follows:

$$\dot{e}(t) = \dot{x}(t) - \dot{\hat{x}}(t) = Ae(t) - LCe(t) \tag{27}$$

L is chosen such that the eigenvalues of $A - LC$ are in the left half of the complex plane, ensuring that the error $e(t)$ converges to zero.

To determine the observer gain L, the Ackermann's formula is used, which gives

$$L = K(A, C) = (A^T - \lambda I)^{-1} CT \tag{28}$$

where λ is a scalar chosen such that the real part of λ is negative, ensuring stability, and T is a matrix that relates the desired eigenvalues of $A - LC$ to the eigenvalues of A.

3.3. Integral State Feedback Control

To ensure that the control target aligns with the set parameters, integral state feedback is employed. This control strategy is particularly effective in systems where the control objectives require the elimination of steady-state errors and the maintenance of desired closed-loop performance characteristics [15].

Integral state feedback is a control technique that integrates the error between the desired output and the actual output of a system over time. This integration process accumulates the error, which is then used to adjust the control input in a way that ensures the system output converges to the desired value, regardless of the initial conditions or disturbances.

$$\begin{cases} \begin{bmatrix} \dot{x} \\ \dot{\omega} \end{bmatrix} = \bar{A} \begin{bmatrix} x \\ \omega \end{bmatrix} + \bar{B} \begin{bmatrix} u \\ 0 \end{bmatrix} \\ y = \bar{C} \begin{bmatrix} x \\ \omega \end{bmatrix} \end{cases}, \tag{29}$$

where $\bar{A} = \begin{bmatrix} A & 0 \\ -C & 0 \end{bmatrix}, \bar{B} = \begin{bmatrix} B \\ 0 \end{bmatrix}, \bar{C} = \begin{bmatrix} C & 0 \end{bmatrix}$. Pole placement is used to calculate the control parameter as follows:

$$P = \lambda(\bar{A} - \bar{B}F), \tag{30}$$

where P is the design value and $F = \begin{bmatrix} F_0 & F_2 \end{bmatrix}$ are the control parameters.

Figure 6 shows the system block, and he Bode diagram of the system is shown in Figures 7 and 8.

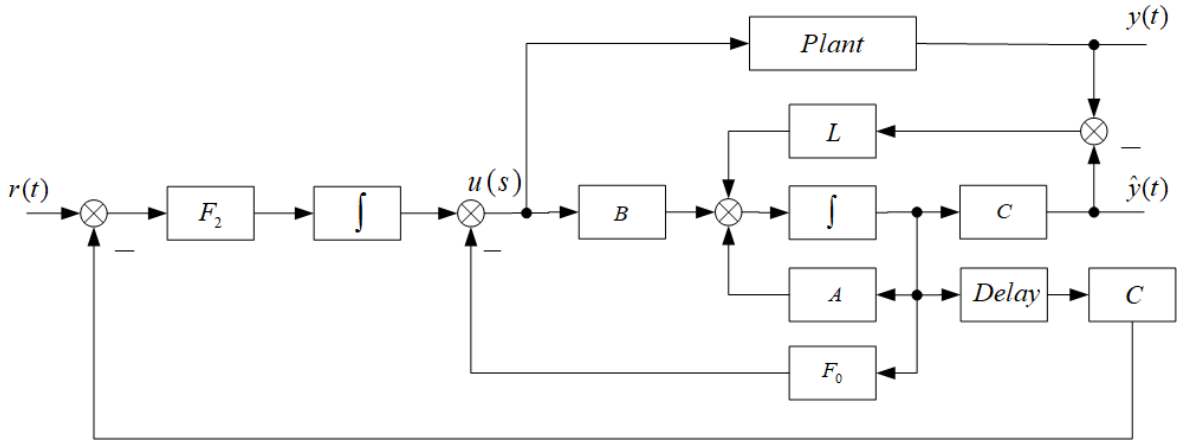

Figure 6. Block of SFC.

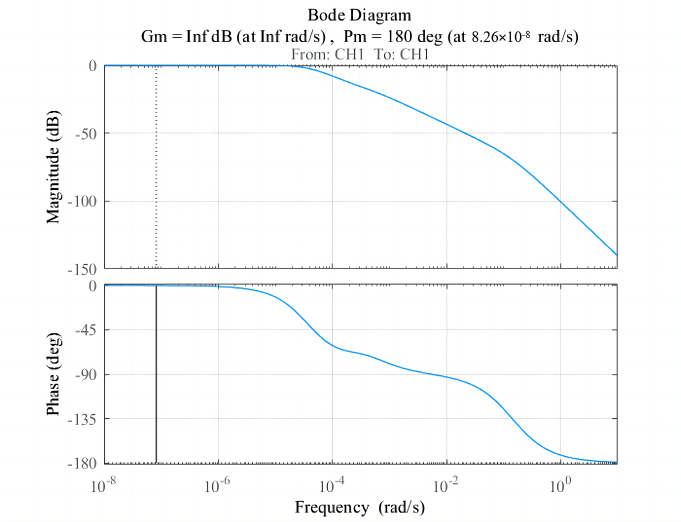

Figure 7. Bode of SFC (CH1 to CH1).

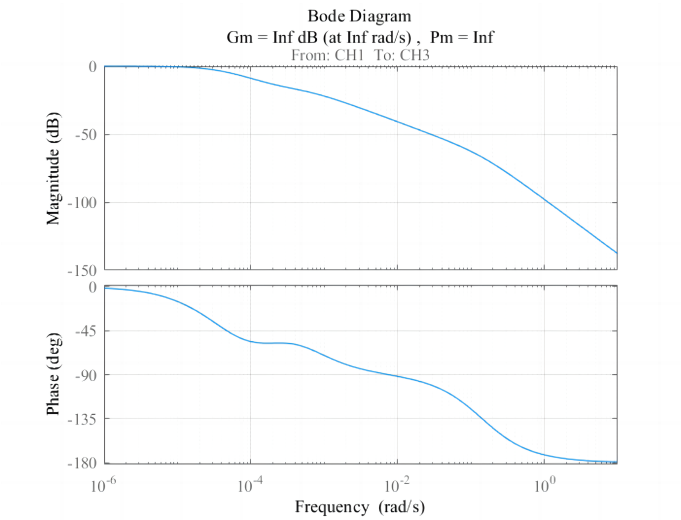

Figure 8. Bode of SFC (CH3 to CH3).

3.4. Target Tracking Control

The individual outputs of the distributed temperature control system may exhibit different responses to step or distance inputs due to errors in system identification. To minimize these discrepancies, one output is designated as the primary target, with the others set to follow this lead output. A two degrees of freedom (2DOF) state feedback control is designed to track this target output. Assuming the second output is chosen as the target, the relevant matrices are defined as follows:

$$D = \begin{bmatrix} 1 & 0 \\ 0 & 0 \end{bmatrix}, \tag{31}$$

In order to facilitate the design of temperature gradient, the difference value between the target and the follower are set as the reference value and a matrix like the follower equation is needed.

$$T = \begin{bmatrix} 1 & -1 \\ 0 & 1 \end{bmatrix}, \tag{32}$$

Figure 9 shows the system block and the Bode diagram of the system is shown in Figures 10 and 11.

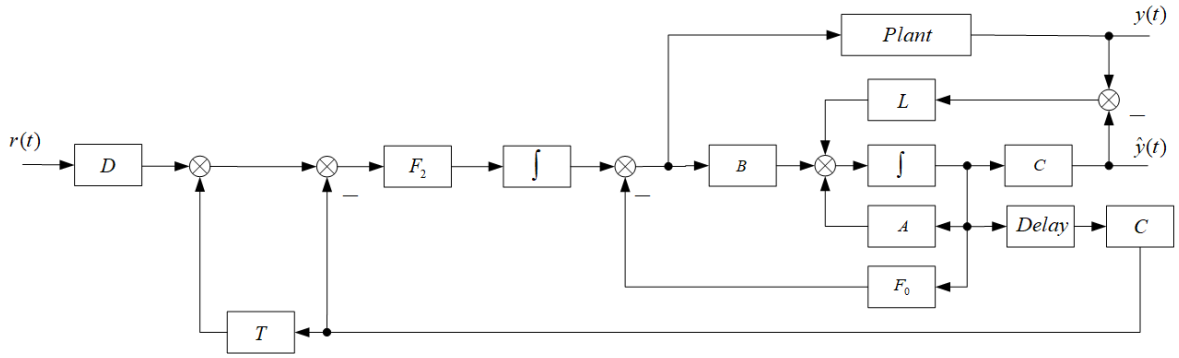

Figure 9. Block of TT SFC.

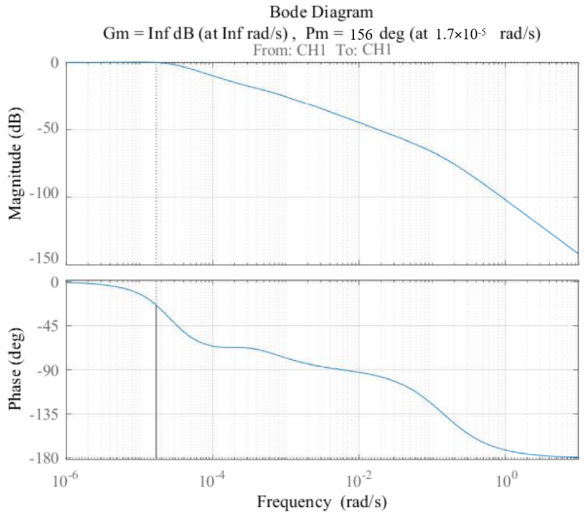

Figure 10. Bode of TT SFC (CH1 to CH1).

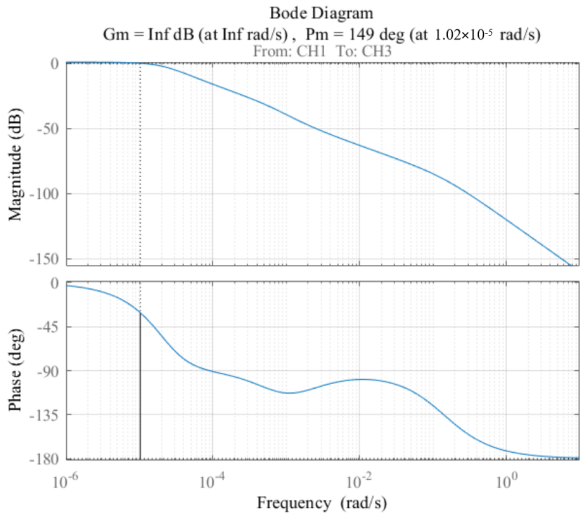

Figure 11. Bode of TT SFC (CH1 to CH3).

3.5. State Feedback and Feed-Forward Control

Traditional closed-loop temperature control systems often struggle to simultaneously optimize response speed and stability. During multi-channel control, achieving temperature stability within the desired range is challenging due to coupling effects. To address this, it is essential to incorporate feed6forward loops into the other channels, which can help reduce response times and minimize the discrepancies between channel outputs [16].

The objective of the feed-forward controller is to design $u(t)$ such that the output $y(t)$ tracks the desired reference trajectory $r(t)$, even in the state vector $\dot{x}(t)$.

Reference trajectory feed-forward:

$$u_{ff}(t) = H_0 r(t) \tag{33}$$

where H_0 is the reference feed-forward gain matrix.

Disturbance feed-forward:

$$u_{ffd}(t) = F_1 \dot{x}(t) \tag{34}$$

where F_1 is the disturbance feed-forward gain matrix.

Total feed-forward control input:

$$u(t) = u_{ff}(t) + u_{ffd}(t) = H_0 r(t) + F_1 \dot{x}(t) \tag{35}$$

Closed-loop system with feed-forward control:

$$u(t) = -Kx(t) + u(t) \tag{36}$$

where K is the state feedback gain matrix.

Closed-loop system dynamics:

$$\dot{x}(t) = A(I - BK)x(t) + B(H_0 r(t) + F_1 d(t)) \tag{37}$$

Feed-forward control, when combined with state feedback, enhances the system's tracking performance and disturbance rejection capabilities. The design of feed-forward gains H_0 and F_1 requires consideration of system performance specifications and potential constraints.The parameters for the feed-forward control are adjusted as follows:

$$H_0 = -\{C(A - BF_0)^{-1}B\}^{-1}D, \tag{38}$$

$$F_1 = C(A - BF_0)^{-1}B, \tag{39}$$

Figure 12, the Bode diagram of the system is shown in Figures 13 and 14.

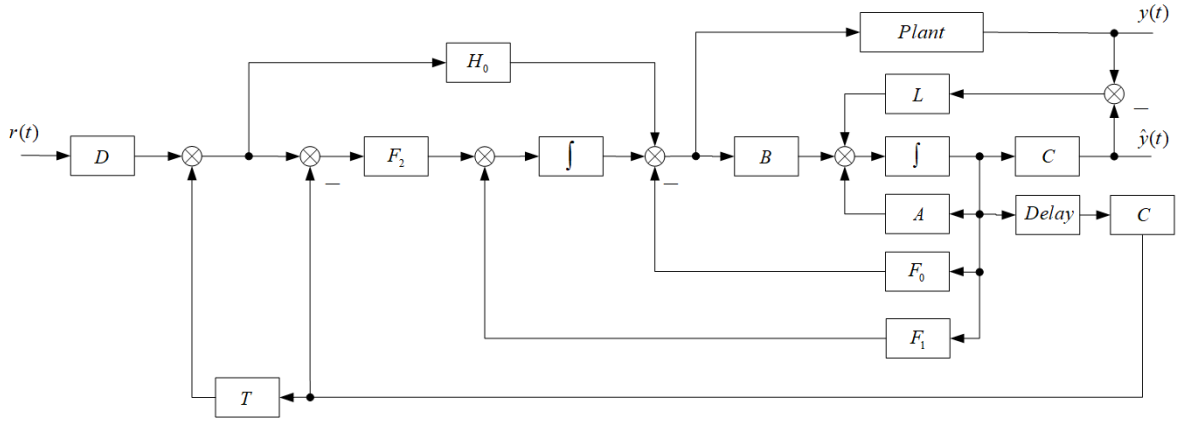

Figure 12. Block of TT 2DOF SFC.

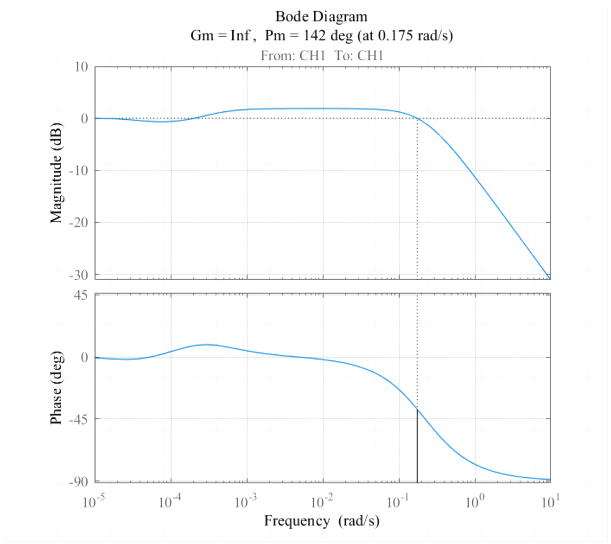

Figure 13. Bode of TT 2DOF SFC (CH1 to CH1).

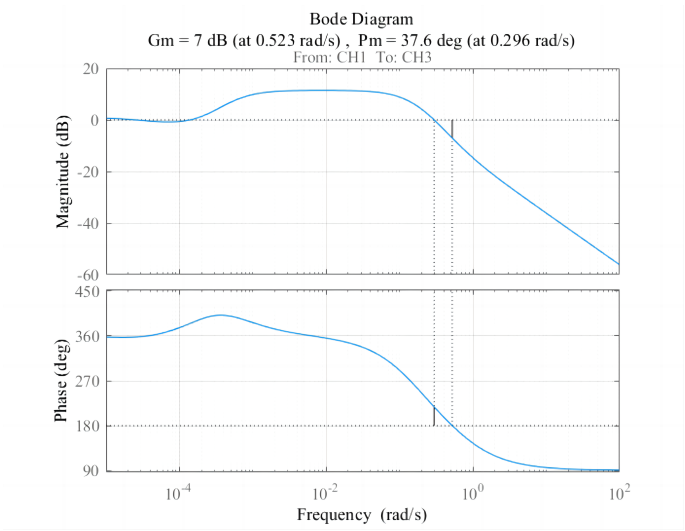

Figure 14. Bode of TT 2DOF SFC (CH1 to CH3).

4. Simulation Result

The results presented were derived from simulations of a DIDO system. These analyses were systematically conducted using Python 3.8 on a acer computer, made in China, equipped with an Intel Core i5 1.8 GHz CPU and 8 GB of RAM.

To evaluate the effectiveness of various control algorithms, a simulated step input signal ranging from 100 to 101 was utilized. The differences in response time and overshoot magnitude between the output responses of the observed system were analyzed.

The traditional PI control simulation was conducted using the parameters detailed in the Table 1, which were configured using the Ziegler–Nichols (ZN) method. The results are depicted in the Figures 15–17: the upper graph illustrates the output results for both channels, while the lower graph compares the differences in their output responses.

Table 1. PI parameter.

	Kp	**Ki**
ch1	6.8	0.0056
ch2	9.2	0.0055

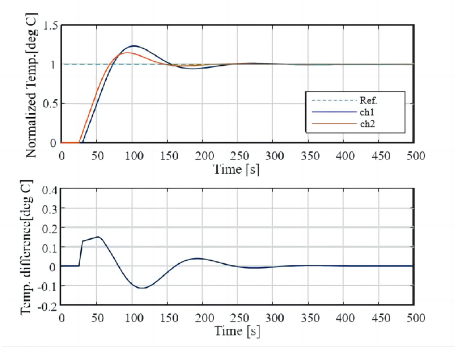

Figure 15. Step response of PI Control.

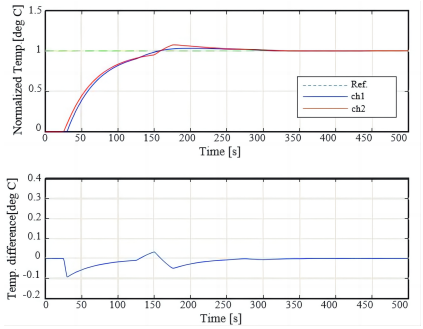

Figure 16. Step response of SFC Control.

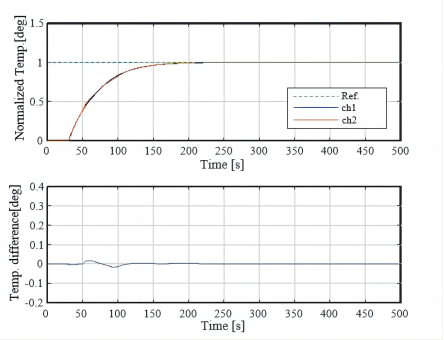

Figure 17. Step response of SFC Control.

The simulation results indicate that the control system's response time is 125 s, the maximum overshoot is 30%, the maximum error between the two output quantities is 0.15 °C, and the error reduction time is 170 s. It is observed that, due to coupling effects, traditional PI control parameter design methods struggle to eliminate overshoot.

For temperature control, the traditional state feedback control (SFC) was implemented as detailed in the table below, and the simulation results are presented in the accompanying figure. These results show that the SFC control system has a response time of 120 s, with no maximum overshoot (0%), a maximum error between the two output quantities of 0.1 °C, and an error reduction time of 162 s. The results demonstrate that SFC effectively reduces system coupling, leading to a notable decrease in overshoot. However, due to the inherent different delay times in the two channels, a discrepancy between the two output quantities persists.

$$Q = [-0.01 - 0.01 - 0.01 - 0.01] \tag{40}$$

$$P = [-0.1 - 0.1 - 0.1 - 0.1 - 5000 - 5000] \tag{41}$$

The temperature control utilizing the SFC method proposed in this paper is detailed in the table provided as Table 2, and the corresponding simulation results are depicted in

the accompanying figure. The simulation outcomes reveal that the response time of this control system is 119 s, with a maximum overshoot of 0%. Additionally, the maximum error between the two output quantities of the system is recorded at 0.04 °C, and the error reduction time is 98 s. The results indicate that the proposed SFC method effectively reduces system coupling. Furthermore, by incorporating a tracking loop and a feed-forward loop, the method significantly mitigates the impact of varying delay times between channels, thereby reducing the error between the two output quantities.

Table 2. Three control simulation methods.

	Response Time	Overshoot	Difference	Difference Time
PI	125	30%	0.15 °C	170 s
SFC	120	0%	0.1 °C	162
TT 2DOF SFC	119	0%	0.04 °C	98

5. Experiment Result

The experimental outcomes for the PI and SFC control systems are as Figures 18 and 19. The Data shows in Table 3 for the PI control system, the response time is recorded at 132 s, the maximum overshoot is 26%, the maximum error between the two output quantities is 0.23 °C, and the error reduction time is 147 s. Consistent with the simulation results, the system experiences notable overshoot and output errors, attributed to coupling and delay issues. Conversely, the SFC control system demonstrates a response time of 108 s, a maximum overshoot of 3%, a maximum error between the two output quantities of 0.21 °C, and an error reduction time of 106 s. The experimental findings are largely in agreement with the simulation results. In comparison to traditional design methods, the SFC approach significantly reduces overshoot and enhances the system's output accuracy.

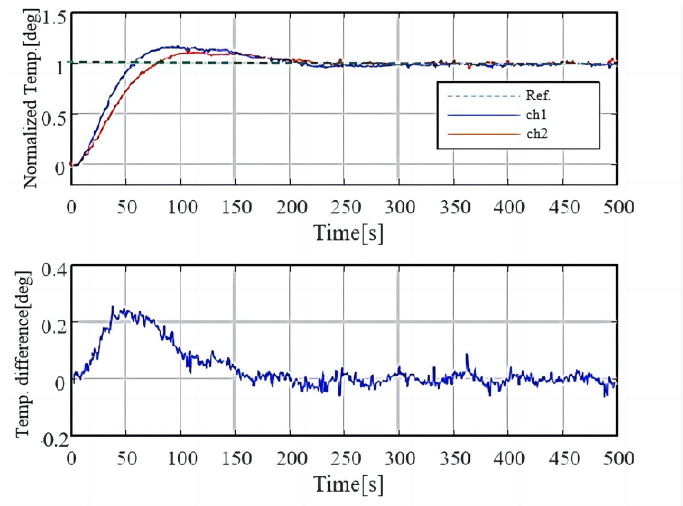

Figure 18. Step response of PI control for experiment.

Table 3. Two control experiment methods.

	Response Time	Overshoot	Difference	Difference Time
PI	132	26%	0.23 °C	147 s
TT 2DOF SFC	108	3%	0.21 °C	106 s

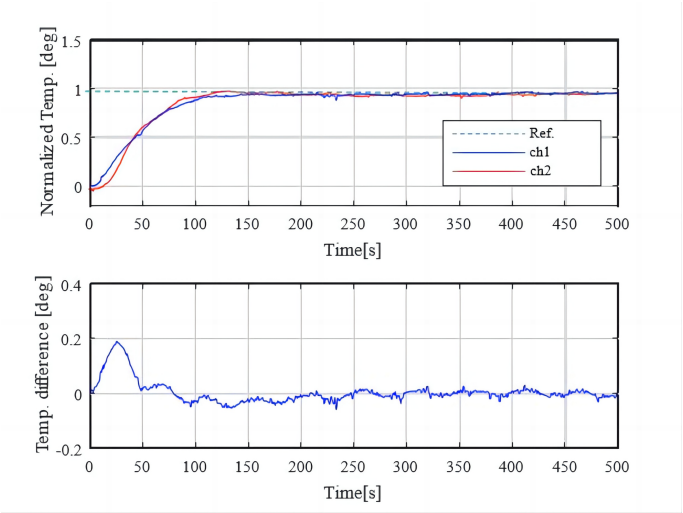

Figure 19. Step response of TT 2DOF SFC control for experiment.

6. Conclusions

This paper presents a significant advancement in the field of control systems with the introduction of a TT 2DOF SFC system. The importance of this research lies in its potential to revolutionize the way we approach target tracking and control performance, both of which are critical in a wide array of applications from industrial automation to aerospace and biomedical engineering. The achievement in this research is multifaceted, as detailed below.

Enhanced Performance: The proposed system demonstrates a marked improvement in dynamic response and steady-state accuracy. The comparative simulations and experiments with a PID system highlight an 18% improvement in response time and a 23% reduction in overshoot. These enhancements are not just numbers but represent tangible benefits in real-world applications, such as faster and more accurate processing in manufacturing or more precise environmental controls in scientific research.

Precision Control: The significant reductions in temperature difference and time to reach set temperatures showcase the system's ability to achieve precise control. This level of precision is crucial in applications where minor deviations can lead to significant outcomes, such as in the pharmaceutical industry for drug synthesis or in laboratories for accurate experimental results.

Simplified Design Process: This study concludes that the SFC system not only enhances control performance but also simplifies the design process. By simplifying the design and implementation of control systems, this research makes sophisticated control strategies more accessible to a broader range of engineers and researchers, potentially leading to a surge in innovation.

Future Innovations: This paper paves the way for future refinements and the development of microcontroller-based prototypes. This opens up avenues for further research and practical implementation, encouraging the integration of advanced control systems in various industries.

Interdisciplinary Applications: By improving the fundamental aspects of control systems, this research adds value across multiple disciplines. The principles and methodologies developed here can be adapted and applied in diverse fields, from robotics to energy management systems.

In conclusion, the introduction of the TT 2DOF SFC system is not just an academic exercise but a significant step forward in the practical application of control systems. It represents a commitment to pushing the boundaries of what is possible, to improving the efficiency and effectiveness of technologies that underpin modern society, and to fostering a future where control systems are more responsive, more accurate, and more integrated into the fabric of our lives.

Author Contributions: Conceptualization, Y.J. and W.J.; methodology, S.H.; software, Y.J.; validation, Y.J., Y.X. and Y.L.; formal analysis, W.J.; resources, Y.J.; data curation, Y.J.; writing—review and editing, Y.J. All authors have read and agreed to the published version of the manuscript.

Funding: This research was funded by Yangzhou City Zero-carbon Smart Manufacturing Engineering Technology Research Center and Yangzhou City Marine Engineering Equipment Innovation Consortia.

Data Availability Statement: The raw data supporting the conclusions of this article will be made available by the authors on request.

Conflicts of Interest: The authors declare no conflict of interest.

References

1. Syama , S.; Mohanan, P.V. Microfluidic based human-on-a-chip: A revolutionary technology in scientific research. *Trends Food Sci. Technol.* **2021**, *110*, 711–728. [CrossRef]
2. Zhang, H.; Li, L.; Wang, S.; Sun, X.; Luo, C.; Hou, B. Construction of dentin-on-a-chip based on microfluidic technology and tissue engineering. *J. Dent.* **2024**, *146*, 105028. [CrossRef]
3. Cui, P.; Wang, S. Application of microfluidic chip technology in pharmaceutical analysis: A review. *J. Pharm. Anal.* **2019**, *9*, 238–247. [CrossRef] [PubMed]
4. Steven, A.D.L. Chapter 9—Managing the societal uses of phytoplankton: Technology applications and needs. In *Advances in Phytoplankton Ecology*; Clementson, L.A., Eriksen, R.S., Willis, A., Eds.; Elsevier: Amsterdam, The Netherlands, 2022; pp. 265–297.
5. Ramón-Azcón, J.; Rydosz, A. (Eds.) Chapter 3—Microfluidic technology in organ-on-a-chip applications. In *Human Organs-On-a-Chip*; Academic Press: Cambridge, MA, USA, 2024; pp. 71–104.
6. Hu, X.G.; Zhao, Y.; Peng, Y.; Chen, X.M.; Wang, L.F.; Lin, Z.T.; Zhao, J.; Hu, S. In-situ label-free temperature-compensated DNA hybridization detection with a fiber-optic interferometer and a fiber Bragg grating for microfluidic chip. *Biosens. Bioelectron.* **2023**, *242*, 115703. [CrossRef] [PubMed]
7. Liu, Z.; Sun, D.; Jiang, B.; Shen, L.; Zhou, P.; Gao, C.; Jin, Z.; Liu, X.; Yang, L.; Tan, S. Continuous gradient temperature control of microfluidic chip based on thermoelectric cooler. *Science* **2023**, *234*, 121277. [CrossRef]
8. Farah, J.; Gravel, E.; Doris, E.; Malloggi, F. Direct integration of gold-carbon nanotube hybrids in continuous-flow microfluidic chips: A versatile approach for nanocatalysis. *J. Colloid Interface Sci.* **2022**, *613*, 359–367. [CrossRef] [PubMed]
9. Li, R.; Wang, Z.; Xu, J.; Yuan, W.; Wang, D.; Ji, H.; Chen, S. Design and optimization of hydraulic slide valve spool structure based on steady state flow force. *J. Colloid Interface Sci.* **2024**, *96*, 102568. [CrossRef]
10. Kopp, U.M.; De Mello, J.A.; Manz, A. Chemical amplification: Continuous-flow PCR on a Chip. *Appl. Therm. Eng.* **1998**, *280*, 1046–1048. [CrossRef]
11. Liu, C.; Geva, E.; Mauk, M.; Qiu, X.; Abrams, W.R.; Malamud, D.; Curtis, K.; Owen, S.M.; Bau, H.H. An isothermal amplification reactor with an integrated isolation membrane for point-of-care detection of infectious diseases. *Analyst* **2011**, *136*, 2069–2076. [CrossRef]
12. Ulep, T.H.; Day, A.S.; Sosnowski, K.; Shumaker, A.; Yoon, J.Y. Interfacial Effect-Based Quantification of Droplet Isothermal Nucleic Acid Amplification for Bacterial Infection. *Sci. Rep.* **2019**, *9*, 9629. [CrossRef]
13. Ren, K.; Xie, Y.; Wang, C.; Yan, J.; Shi, Y.; Guo, J.; Guo, J. Application of the fuzzy proportional integral differential (PID) temperature control algorithm in a liver function test system based on a centrifugal microfluidic device. *Talanta* **2024**, *268*, 125330. [CrossRef] [PubMed]
14. Pasand, M.M.S.; Ahmadi, A.A. A generalized nonlinear extended state observer for multi-output Lipschitz systems. *Eur. J. Control* **2024**, *75*, 100906. [CrossRef]
15. Seeber, R.; Tranninger, M. Integral state-feedback control of linear time-varying systems: A performance preserving approach. *Automatica* **2022**, *136*, 110000. [CrossRef]
16. Li, B.; Du, X.; Fan, H.; Liu, Z.; Liu, C. Microgrid inverter control strategy based on augmented state feedback and dynamic feedforward compensation. *Energy Rep.* **2022**, *8*, 723–732. [CrossRef]

Disclaimer/Publisher's Note: The statements, opinions and data contained in all publications are solely those of the individual author(s) and contributor(s) and not of MDPI and/or the editor(s). MDPI and/or the editor(s) disclaim responsibility for any injury to people or property resulting from any ideas, methods, instructions or products referred to in the content.